Sensor and Simulation Notes

Note 270

1 March 1981

# Instrumentation For An Underground Nuclear SGEMP Experiment

R. H. Bonn

Field Command Defense Nuclear Agency
Currently at JAYCOR

PREFACE

Fabrication of the sensors used for the HURON KING underground nuclear SGEMP experiment was accomplished by Messrs. Jon Mellville and Jerry Camilli of EG&G, Inc., and Mr. Joe Fisher of Fisher Electronics. Mr. Tom Summers of Summers Engineering made contributions in the areas of design and sensitivity calculations. The manufacturer's data on the ferrite cores was reproduced with the permission of Ceramic Magnetics, Inc. Radiation noise tests were performed by Drs. Ralph Stahl and Bill Siedler of JAYCOR. Dr. Carl Baum of the Air Force Weapons Laboratory provided many helpful suggestions.

# SECTION 1

# INTRODUCTION

## 1-1 GENERAL.

The HURON KING underground nuclear test was a Department of Defense sponsored nuclear weapons effects test. The test object was a full scale model of the Defense Satellite Communication System III (DSCS III) satellite and was equipped with several DSCS III electronic subsystems including the power system, cryptologic equipment, and engineering model hardware from the DSCS III project. The 2100 pound test object had power applied and was processing commands at zero time.

## 1-2 EXPERIMENT CONFIGURATION.

The experiment configuration was composed of a nuclear device buried 1000 feet underground, a vertical line of sight (VLOS) pipe to the surface, a scatterer, and a vacuum tank which held the test object. The 250 ton steel tank provided a vacuum of $2 \times 10^{-4}$ torr. Minimizing the tank response to extraneous noise was accomplished by coating the tank inside surface with glyptol, suspending a carbon impregnated cotton fabric damper grid inside the tank, electromagnetically isolating the scatterer from the test object, and providing a single inductively loaded ground point between the test object and the vacuum tank.

SECTION 2

GROUNDING AND SHIELDING

2-1 PURPOSE.

The purpose of implementing a grounding and shielding plan on HURON KING was to minimize noise and thus enhance the probability of experiment success. Potential noise sources include EMP, noise from photon illumination of instrumentation/cables, and noise from external sources.

2-2 METHOD.

The following list itemizes the grounding and shielding shot configuration (also see Figure 1).

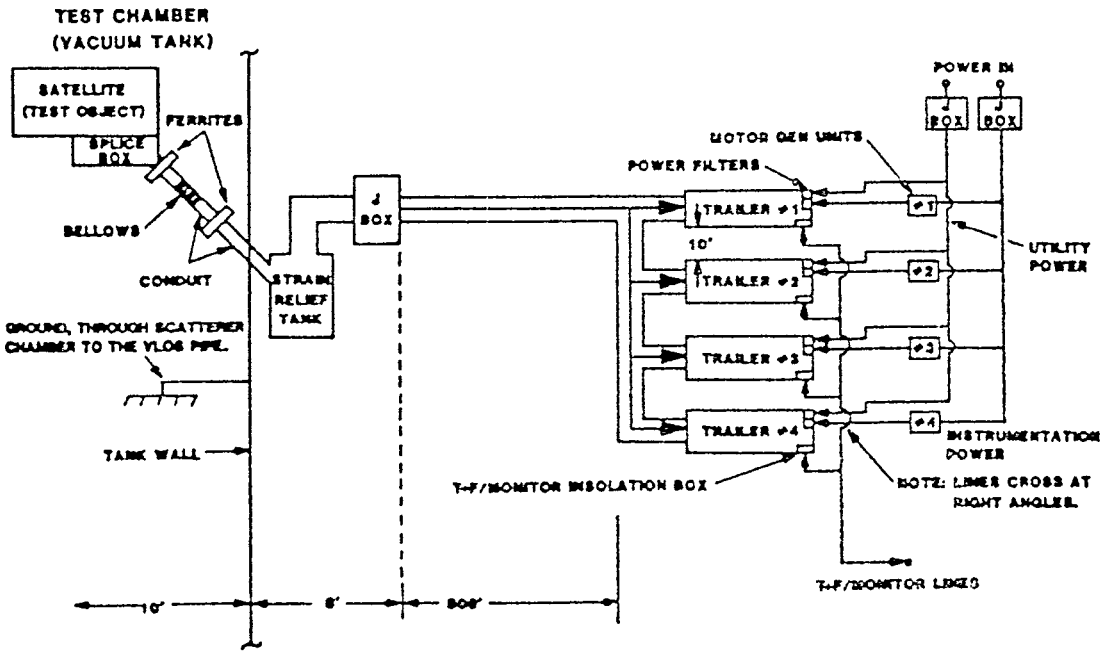


Figure 1. Grounding and shielding configuration

(a) There was a single electrical path from the zero room to the recording trailers. This was provided by the pipe, scatterer chamber, test chamber, splice box, stinger, J-box, and cable bundle.

(b) The overall layout for signal paths forms a tree network with no loops. This required that the SGEMP cables be isolated from all other experiments once they leave the vacuum tank. All external connections to the instrument trailers (except data lines)

were electrically isolated or removed prior to shot time. External fire alarms and phone lines were disconnected. The instrumentation power was isolated by a motor-generator unit and filtered, the utility power was filtered, and the timing and firing and monitor lines were isolated at the trailer wall.

(c) The SGEMP cable run had an external electrically conducting RF shield over its run from the test object to the J-box. This consisted of the splice box, the conduit between the splice box and the tank wall, the conduit from the tank wall to the J-box, and the J-box. All connectors made circumferential grounds and had RF tight backshells. No cables entered the J-box or the trailer without a circumferential ground. Aluminized mylar was not used for cable shielding. Each trailer provided a minimum of 40 decibels attenuation to a plane wave at 1 MHz and had a high quality feed-through panel.

(d) The SGEMP cable run was placed on the ground.

(e) One quarter inch of lead was placed over the cable run to a distance of 200 feet from the line-of-sight pipe.

## SECTION 3

## SGEMP SENSORS FOR HURON KING

### 3-1 SUMMARY OF TECHNIQUES.

This section summarizes the techniques employed in the manufacture of SGEMP sensors for HURON KING. The sensors were designed for a gamma environment of $10^8$ rads/sec and a shock environment of six g's. The standard techniques in construction of SGEMP sensors for a vacuum environment were employed. These include:

(a) All sensor output cables are solid jacketed aluminum coax cables with teflon dielectrics.

(b) There are no connectors at the sensor.

(c) The number of solder joints is minimized, and such connections are shielded where possible.

(d) Where surface emission will effect the measurement, the surface is coated with glyptol or potted in dielectric.

(e) The outer surface of the sensor is either aluminum, glyptol coated, or chemglazed.

The aluminum cables were used because they provided less shielding of the test object, and because they conformed more easily to the topology of the satellite chassis. A summary of the sensors used follows.

### 3-2 B-DOT SENSORS.

The B-dot sensors which found application in the underground nuclear test are listed herewith.

#### 3-2.1 CML-X3F B-Dot Sensor.

This sensor, shown in Figure 2, differs from other CML-X3 sensors (References 1 and 2) in the following ways:

(a) The sensor is mounted on a plate above the ground plane. This plate was tapered to reduce the effect of a sudden change in height in the ground plane. The enhancement of the sensor height above the ground plane was considered in the equivalent area calculations.

(b) Because of space limitations the sensing element was reduced to four centimeters in length. From Reference 3 we can see that with a B-dot loop of this length there is minimal advantage in loading the gap at two points. It was therefore decided to use one load point. This in turn eliminated the 100 ohm coax and the solder joint between the 100 ohm and 50 ohm coax, which meant that no lead was required in this sensor. The base plate was thereby reduced in height to .4 centimeters.

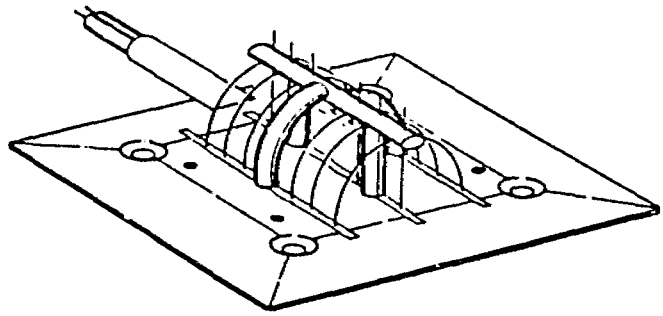

Figure 2. CML-X3F B-dot sensor

The CML-X3F B-dot sensor measures the time derivative of magnetic flux density. The line integral of the electric field around a loop is equal to the surface integral of the time rate-of-change of the magnetic flux density over the area of the loop. Thus the voltage output of the half cylinder over the ground plane is

$$V_c = \oint_\ell \vec{E}\cdot d\vec{\ell} = -\frac{\partial}{\partial t}\oint_s \vec{B}\cdot d\vec{s} = -\frac{\partial B}{\partial t}\frac{\pi a^2}{2}$$

where 'a' is the cylinder radius. Because the sensor output is taken differentially we obtain the sensor output voltage as

$$V_o = 2V_c = \pi a^2 \frac{\partial B}{\partial t}.$$

The radius of the cylinder varies slightly from 'a' because:

(a) The cylinder is composed of wires which have a non-zero (10 mil) diameter.

(b) There is a wire ground fence running the length of the cylinder which decreases the area of the loop by .0316 sq cm.

(c) The cylinder is raised slightly (.4 cm) above the ground plane.

A low frequency equivalent circuit is shown in Figure 3.

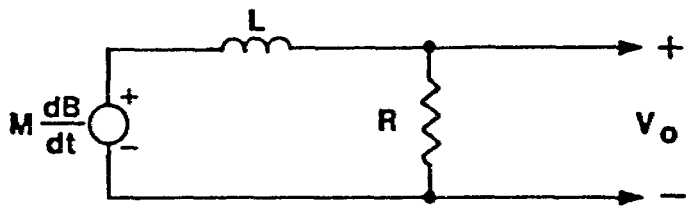


Figure 3. CML equivalent circuit

In the frequency domain the output voltage is

$$V_o(s) = \frac{MsB(s)R_L/L}{s + R_L/L}$$

or, for frequencies where $s << R_L/L$, $V_o(s) = sMB(s)$.

3-2.2 RML-X1 B-Dot Sensor.

This rectangular B-dot sensor (see Figure 4) was designed to measure the time rate-of-change of the magnetic field between the satellite aluminum outer surface and the aluminized mylar thermal blankets. There is a dielectric support which keeps the thermal blanket one sensor radius above the sensing element. The RML-X1 has the same equivalent area, frequency response, specifications, and general design considerations as the CML-X3.

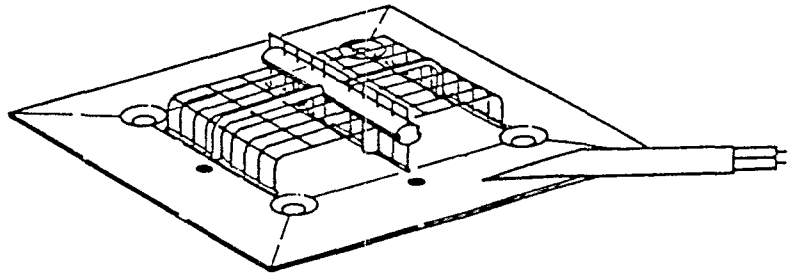

Figure 4. RML-X1 B-dot sensor

3-3 E-FIELD SENSORS.

One of the E-field sensors that has proven useful in underground testing is the PMD-1F, which is a parallel plate E-field sensor.

3-3.1 PMD-1F E-Field Sensor.

This sensor is similar to previous PMD sensors developed at the Air Force Weapons Laboratory, except that the lead shielding was reduced from 250 mils to 20 mils and the output cables were routed along the ground plane. The performance of this sensor is well documented in references 4 and 5. The specifications and theory will be briefly reviewed here.

The PMD-1F E-field sensor is composed of a .5 mil aluminum wire grid suspended above a ground plane. The output voltage of this parallel plate capacitor is sensed across the R-C network as shown in the equivalent circuit (see Figure 5) where $R_2$ is the characteristic impedance of the aluminum output cable. Some distributed capacitance exists across the sensing resistor. This is compensated by a small copper plate inside the sensing resistor box, which adds capacitance across the load. The distributed capacitance is in series with the compensating capacitor, and forms a voltage divider. The output waveform therefore becomes independent of the distributed capacitance across the sensing resistor. The amount of compensating capacitance is not known, but selected by moving the plate until the time domain reflectometer shows a minimum of ringing at the connector.

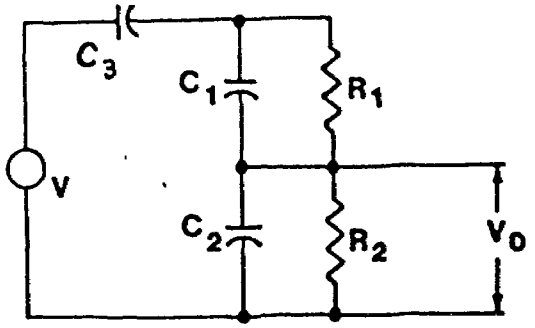


$C_1$ = distributed capacity ($C_1 \ll C_3$)
$C_2$ = compensating capacity (unmeasured)
$C_3$ = sensor capacity (20 pF)
$R_1$ = sensing resistance (5 KΩ)
$R_2$ = load resistance (50Ω)
$V_o$ = output voltage
$V^o$ = input voltage caused by line integral of the electric field between the sensor plates.

Figure 5. Equivalent circuit of the PMD-1F E-field sensor

Applying the equation:

$$V = \int \vec{E} \cdot d\vec{\ell}$$

to the geometry under consideration yields

$$V_o = - E h$$

where h is the effective height of the sensor.

3-4 I-DOT SENSORS.

The sensors which measure time rate of change of current are listed here.

3-4.1 OMM-4 I-Dot Sensor.

The OMM-4 (Outside Moebius Mutual) I-dot sensor (Figure 6) uses the same principles as previous OMM sensors have used (References 6 & 7). It was built to measure the time derivative of current on the stinger (7.5 inch i.d. cable conduit). Because of the vacuum environment, ionized air cannot short out the signal. Therefore, the sensor volume was not potted solid; it was instead coated with 5 mils of glyptol.

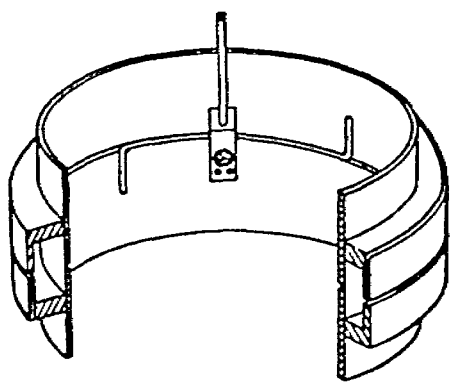

Figure 6. OMM-4 I-dot sensor

The OMM-4 I-dot sensor is designed to be part of a cylindrical conduit. The sensing volume is an additional cylindrical housing which circumscribes the conduit housing. The voltage across the sensing gap is sampled at four points and delivered differentially through two 50 ohm coaxial cables. A low frequency equivalent circuit is shown in Figure 7.

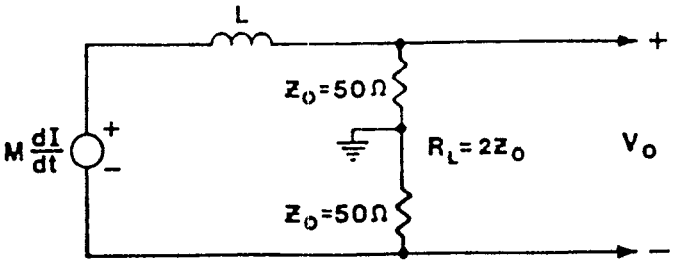


Figure 7. OMM-4 equivalent circuit

The open circuit voltage, $V_0$, is obtained by integrating $B_{\phi\ avg.}$ over a cross section of the sensor volume and multiplying by the number of loop turns. This gives:

$$V_0 = M\frac{dI}{dt}$$

for frequencies below the upper 3 decibel points. The Laplace transform of the output voltage is:

$$V_0(s) = \frac{sMR_L I}{sL + R_L}$$

from which it may be observed that the sensor is self integrating when: $|s| >> R_L/L$.

3-4.2 SMM-X1 I-Dot Sensor.

The SMM-X1 (Side Moebius Mutual) I-dot sensor (Figure 8) is designed to measure current on the satellite model solar array support arm. The gap was placed on the side of the sensor for physical convenience. The sensor volume was coated with 5 mils of glyptol. The sensor housing is bolted to the ground plane with the solar array support arm passing through an aperture in the center of the sensor. The voltage across the sensing gap is sampled at four points and delivered differentially through two 50 ohm coaxial cables.

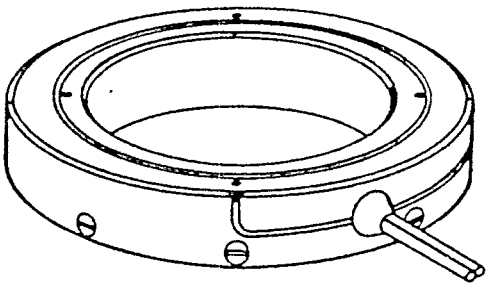

Figure 8. SMM-X1 I-dot sensor

The SMM-X1 I-dot sensor is similar to the OMM sensors. A brief description of the I-dot sensor theory is given in section 3.4.1 of this report with more detail in references 6 & 7.

3-5 RADIATION HARDENED CURRENT SENSORS.

Two basic types of current sensors were developed. The SCI (Split Core Current) sensor series are clamp on current sensors designed to measure current on cable bundles. These sensors use a coaxial cable as their sensing element. The ICI-X3 (Inside Core Current) sensor series are solid core current sensors designed to have low insertion impedance and to measure pin level currents. These sensors use a bifilar transmission line as the sensing element.

3-5.1 Purpose.

The radiation hardened current sensors were developed to measure current in a photon/vacuum environment for the underground nuclear test HURON KING.

3-5.2 Design Constraints.

(a) Radiation: To minimize the noise from radiation the following features were included:

(1) Differential output.

(2) Aluminum solid jacket, teflon dielectric, coax output leads.

(3) All external surfaces are either aluminum, glyptol coated, or chem-glazed (i.e., use of low Z materials).

(4) Elimination of connectors at the sensor.

(5) Some internal lead shielding.

(6) Elimination of internal equalizing networks at the sensor.

(b) Electrical: The following comprise some of the electrical design constraints:

(1) Capability to measure frequencies as low as 4 Khz.

(2) Capability to measure frequencies as high as 300 Mhz.

(3) Capability to measure currents with d.c. components as large as 18 amperes without saturating.

(4) Insertion impedance of less than 10 milliohms.

3-5.8 Method of Construction.

The current sensor (Figure 9-A) is composed of a ferrite core, a transmission line sensing element, and a slotted aluminum housing. Because the sensor was to be used in a vacuum/radiation environment, all voids were potted and all high Z (high atomic number) material surfaces were coated with a low Z material such as glyptol. Additionally no connectors and no compensation components were used in the sensor design. The cross section in Figure 9-B shows a glyptol coated ferrite core wrapped in electrical tape. A transmission line (75 mil Al coax shown) is wrapped around the sensor core and connected half way through the turns in a moebius configuration (Figure 9-C).

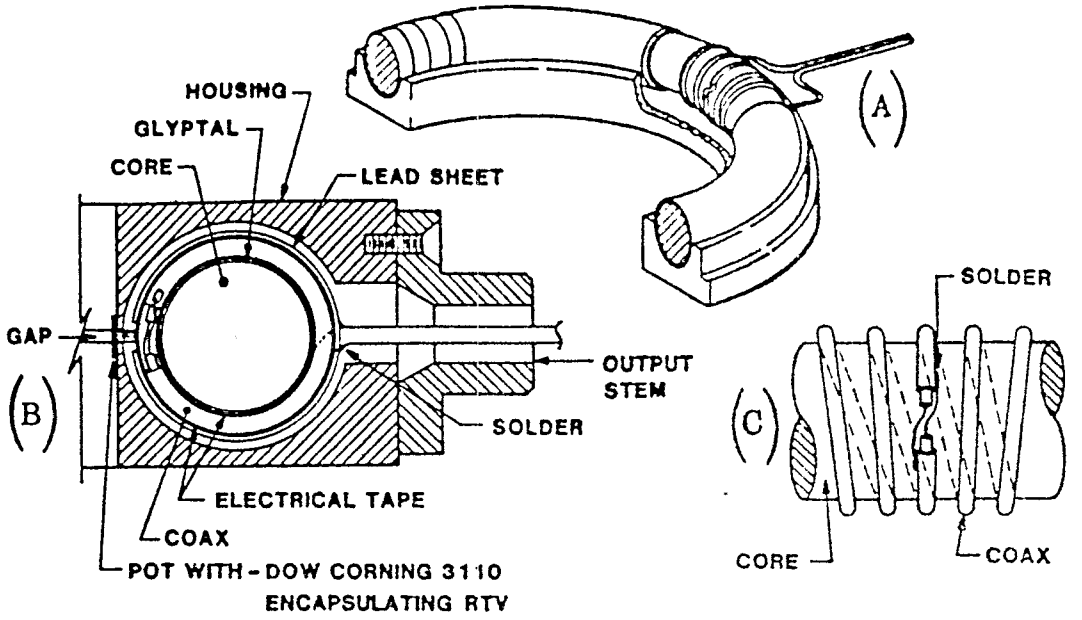


Figure 9. Split core current sensor

The coax is grounded to the case where the turns are completed, and then grounded continuously until they exit the sensor. The winding portion of the coax is covered with shrink tubing and the area between the windings is filled with RTV. This entire assembly is then wrapped in electrical tape and 10 mils of lead. After the gap has been cut in the lead, the assembly is placed in the bottom half of the housing and the top half of the housing is silver epoxied on. The sensor gap is then filled with RTV. This RTV is allowed to extend outside the gap to reduce the space charge in the area of the gap. With the exception of the gap area the sensor is then painted with chemglaze.

The ICI-X3 sensors utilized a 50 ohm bifilar transmission line instead of a coaxial one. This was done because the coax was too large for this small diameter sensor. It was empirically determined that it was not necessary to distribute the winding of either transmission line across the entire core. The split ends of the core were polished smooth to minimize the air gap. Sensors built without the air gap showed only a 3% improvement in the lower 3 decibel point.

3-5.4 Current Sensor Parameters.

The current sensors are transformers with a one turn primary. The use of a transmission line with a moebius gap as the secondary winding provides a differential output with a maximum suppression of radiation noise (Ref 9), and improves the high frequency response by reducing the physical length of the winding.

Two transmission lines will be discussed. The first is the coaxial (or bifilar) cable that is the 'transformers' secondary winding. The second is the transmission line

composed of one of the leads from the first transmission line and the sensor housing. Because the coax is grounded where the turns are completed, the second transmission line acts as a shorted quarter wave transmission line and directly effects the upper 3 db frequency response.

3-5.4.1 Equivalent Circuits. The equivalent circuit of the current probes is seen in Figure 10. The one turn primary winding is the wire under test, while the n turns are the sensor windings. Leakage flux and winding resistances have not been included in the equivalent circuit because they have been empirically determined to be very low. The magnetizing inductance, $L_m$, is the constant of proportionality which relates the primary input current, the number of primary turns, and the flux induced by the primary which links the secondary windings. The magnetizing inductance is significant at low frequencies.

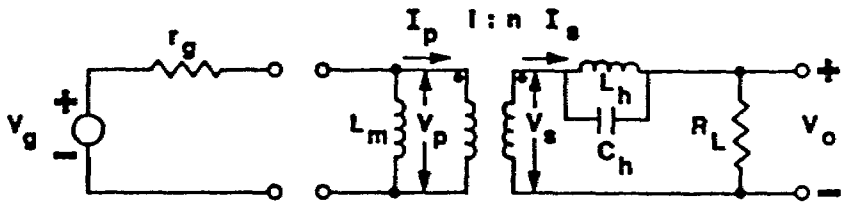


Figure 10. Current probe equivalent circuit

The parallel resonant circuit consisting of $L_h$, and $C_h$ determines the high frequency response of the sensor. These lumped elements represent the shorted quarter wave transmission line discussed in paragraph 3-5.4. Observe that doubling the number of turns doubles the length of the shorted quarter wavelength transmission line and thus reduces the high frequency response by a factor of two.

3-5.4.2 Transfer Function. In the frequency domain the ideal transformer equations are:

$$V_s(s) = nV_p(s)$$

$$I_s(s) = I_p(s)/n$$

$$Z_{in} = \frac{1}{n^2} R_L$$

The midfrequency voltage transfer function is:

$$\frac{V_o(s)}{V_g(s)} = \frac{R_L}{n(r_g + R_L/n^2)}$$

The low frequency voltage transfer function is:

$$\frac{V_o(s)}{V_g(s)} = \frac{R_L}{n(r_g + R_L/n^2)} \left( \frac{1}{1 + \frac{r_g R_L}{sL(n^2 r_g + R_L)}} \right)$$

The high frequency voltage transfer function is:

$$\frac{V_o(s)}{V_g(s)} = \frac{nR_L(1 + s^2L_hC_h)}{sL_h + (n^2r_g + R_L)(1 + s^2L_hC_h)}$$

where the resonant frequency of the parallel resonant circuit composed of $L_h$ and $C_h$ is inversely proportional to the length of the winding. From the transfer functions the following observations may be made.

Increasing the number of turns:

(a) decreases the output.

(b) lowers the lower 3 db point by $n^2$.

(c) lowers the upper 3 db point by n.

3-5.4.3 Transfer Impedance. When these current probes are terminated in the coax characteristic impedance, their transfer impedance over the flat portion of the curve is:

$$Z_t = \left.\frac{V_o}{I_{in}}\right|_{f_L < f < f_U} = \left.\frac{R_L}{n}\right|_{f_L < f < f_U}$$

where

$f_L$ = frequency of lower 3 db point.

$f_U$ = frequency of upper 3 db point.

$R_L$ = 100 ohms

3-5.4.4 Insertion Impedance. The insertion impedance is the impedance introduced into the line under test by the sensor. As previously noted this impedance is:

$$Z_{in} = \left.Z_L/n^2\right|_{f_L < f < f_U}$$

In many applications more than one wire is being measured by the current probe. The effect these additional wires have on the impedance inserted into a particular wire under test may be important. The addition of more terminated wires through the current probe (each with one effective turn) has the effect of adding an impedance in parallel with the n turns of the sensor which equals the load impedance of this new wire. Thus, the insertion impedance introduced into a single wire decreases with the addition of terminated loops through the probe. In this case the total insertion impedance is

$$Z_{ins} = \frac{1}{\frac{1}{Z_{in}} + \frac{1}{Z_1} + \frac{1}{Z_2} \cdots + \frac{1}{Z_n}}$$

where $Z_1$, $Z_2$, . . . . , Z are the impedances introduced by the additional wires. Note that if these wires are electrically long these impedances will be complex. Also note

that when a cable bundle shield is electrically thin at the frequency of interest, some impedance from a current probe around the entire bundle will be inserted into each interior wire.

3-5.5 Large Current Effects.

The introduction of a few amperes of direct or pulse current shifts the hysteresis loop and decreases the low frequency response of the probe. From the manufacturer's data (Figure 11) it can be seen that a core whose average circumference is 1.8 inches saturates at approximately 8 amperes. Short of saturation, a direct current causes an upward shift in the lower 3 decibel point. This result is illustrated in Figure 12 where small signal magnitude versus frequency is plotted for an ICI-X3C current probe for various values of direct current.

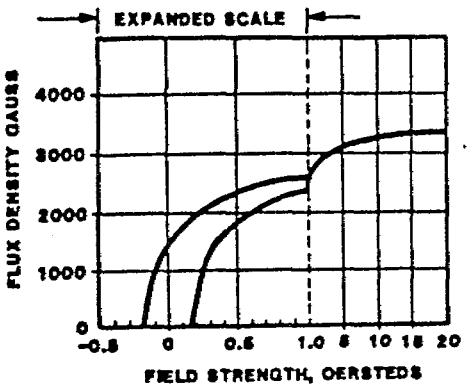


Figure 11. Hysteresis loop for core material

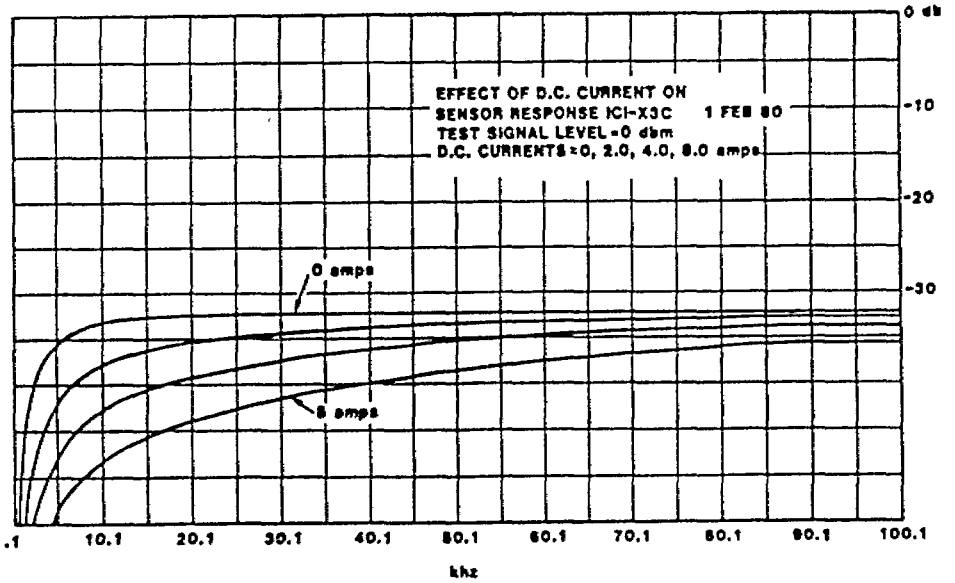


Figure 12. Sensor response dependence on current

In Figure 13 two pulses are superimposed on the top trace. When the input to the sensor was a 2 ampere square wave, the R/L droop is depicted in the top curve. The superimposed curve is the result of a 4 ampere input signal (with oscilloscope vertical gain set to 1/2 the first sweep amplitude). Note that after approximately two microseconds the curves diverge as the magnetizing inductance changes. The magnetizing inductance is dependent on pulse voltage, temperature, and core resistivity. When these sensors are used for current pulses which exceed one microsecond in duration and four amperes in amplitude, caution must be exercised in interpreting the results.

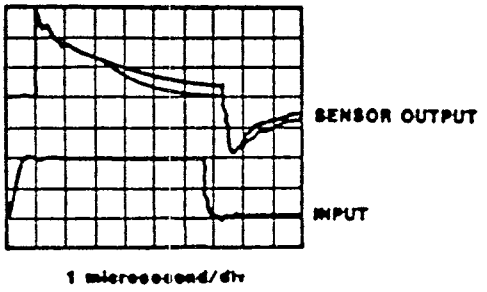


Figure 13. Large Signal Effects

SECTION 4

# SENSOR SPECIFICATIONS

## 4-1 GENERAL.

Specifications for a number of the sensors discussed in the previous section are set forth below. These are the CLM-X3F and RML-X1 B-dot sensors, the PMD-1F E-field sensor, and the OMM-4 and SMM-X1 I-dot sensors. Table 1 summarizes information on a number of current sensors. Figures 14 through 24 show the frequency response exhibited by these current sensors. Corrections for cable length were made in accordance with the attenuation per unit length of 50 Ω cable (Figure 25).

### 4-1.1 CML-X3F and RML-X1 B-Dot Sensors

These sensors are described in paragraphs 3-2.1 and 3-2.2. Specifications are:

Equivalent area ($A_{eg}$) = $5 \times 10^{-4}$ $m^2$
Derivative frequency response < 330 MHz
Self inductance = 12 nH
Output is differential with 100 mil aluminum coaxial cables

### 4-1.2 PMD-1F E-Field Sensors

This sensor described in paragraph 3-2.1 has the following specifications:

Equivalent height = 0.618 cm
Frequency response = 1.6 MHz to 3.5 GHz (3 dB points for integral response)
Capacitance = 20 pF
Risetime ($t_r$, 10-90%) = 0.1 ns
Delay time = 1.5 ns
Maximum output = 25 V

### 4-1.3 OMM-4 I-Dot Sensor

Specifications for the OMM-4 I-dot sensor, described in paragraph 3-4.1, are:

Mutual inductance = 2 nH
Self inductance = 4 nH
Frequency response > 700 MHz
Risetime ($t_r$, 10-90%) < 0.5 ns
Output is differential with two 50 Ω coax cables

### 4-1.4 SMM-X1 I-Dot Sensor

Specifications for this sensor, which is similar to the OMM sensors, are:

Mutual inductance = 2 nH
Self inductance = 4 nH
Frequency response > 800 MHz
Risetime ($t_r$ 10-90%) = 0.42 ns
Output is differential with two 50 Ω coax cables.

Table 1. Current sensor parameters.

| Nomenclature | Sensor Type | Number of Windings | Number of Turns | Transfer Impedence (ohms) | Insertion Impedence (ohms) | Frequency Response Lower 3dB (kHz) | Frequency Response Upper 3dB (MHz) | Dimensions Aperture (cm) | Dimensions Outside Dia. (cm) | Dimensions Height (cm) |
|---|---|---|---|---|---|---|---|---|---|---|
| ICI-X3A | Differential Current, Solid Core | 5 | 10 | 10 | 1 | 84.5 | 200 | 1 | 3.2 | 1.63 |
| ICI-X3B | Differential Current, Solid Core | 10 | 20 | 5 | .250 | 21 | 90 | 1 | 3.2 | 1.63 |
| ICI-X3C | Differential Current, Solid Core | 20 | 40 | 2.5 | .0625 | 4 | 54 | 1 | 3.2 | 1.63 |
| ICI-X3D | Differential Current, Solid Core | 40 | 80 | 1.25 | .0156 | 1.35 | 30 | 1 | 3.2 | 1.63 |
| SEC-X1 | Single Ended Current, Solid Core | 20 | 20 | 2.5 | .125 | 10.75 | 66 | 1 | 3.2 | 1.63 |
| SCI-X1 | Differential Current, Split Core | 5 | 10 | 10 | 1 | 83 | 500 | 2 | 7.9 | 2.7 |
| SCI-X2 | Differential Current, Solid Core | 5 | 10 | 10 | 1 | 85 | Not Measured | 3 | 8.9 | 2.7 |
| SCI-X3 | Differential Current, Split Core | 5 | 10 | 10 | 1 | Not Measured | Not Measured | 10 | 15.9 | 2.7 |
| ICI-X2 | Differential Current, Solid Core | 5 | 10 | 10 | 1 | | | 10 | | |
| MEAS #110 | Differential Current, Solid Core | 10 | 10 | 5 | .5 | | | | | |
| MLAS #122C | Differential Current, Solid Core | 70 | 70 | .71 | .010 | | | | | |
| F32-8 | Differential Current, Solid Core | 20 | 40 | 2.5 | .0625 | | | 1 | 4.2 | 1.19 |
| F32-9 | Differential Current, Solid Core | | | | | 83 | 194 | | | |

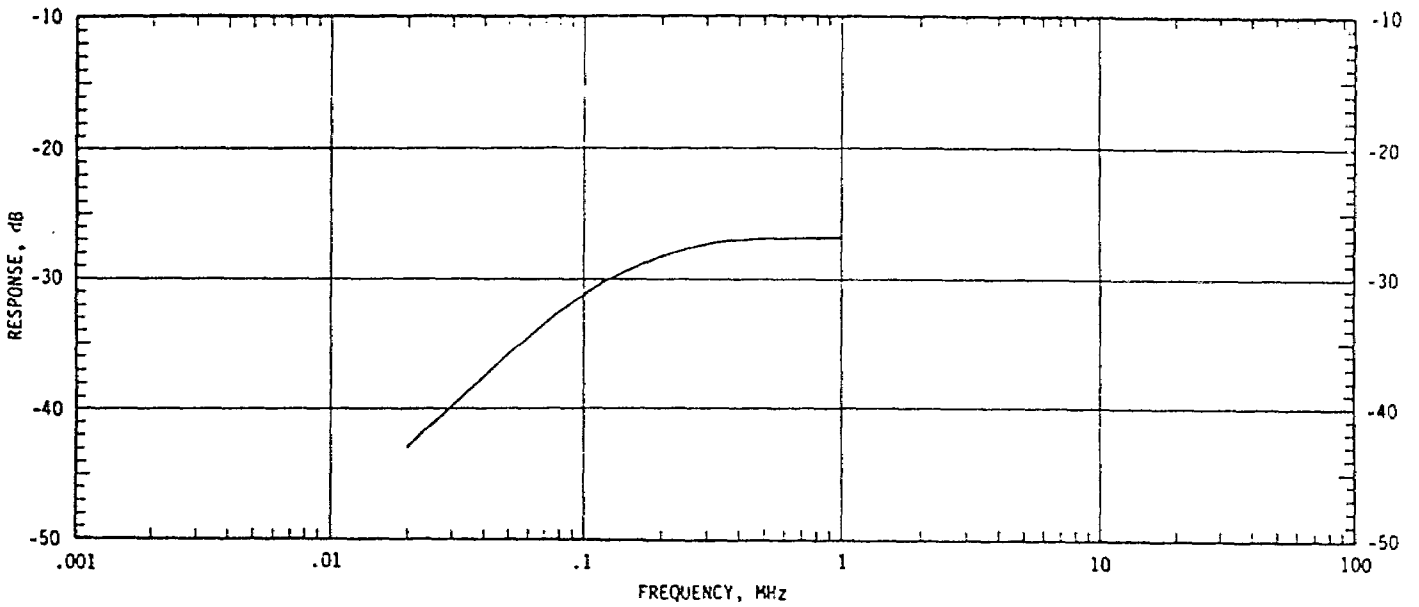


Figure 14. Frequency response for SCI-X2 current sensor (not corrected for cable length).

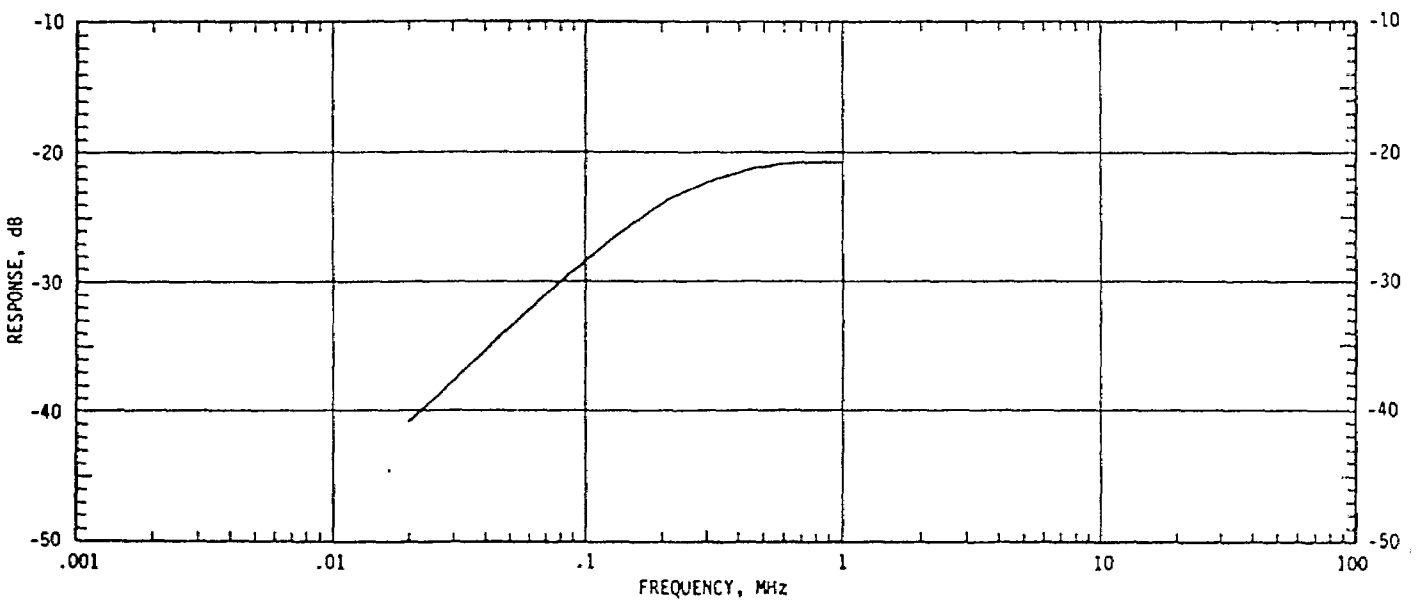


Figure 15. Frequency response for ICI-X2 current sensor (not corrected for cable length).

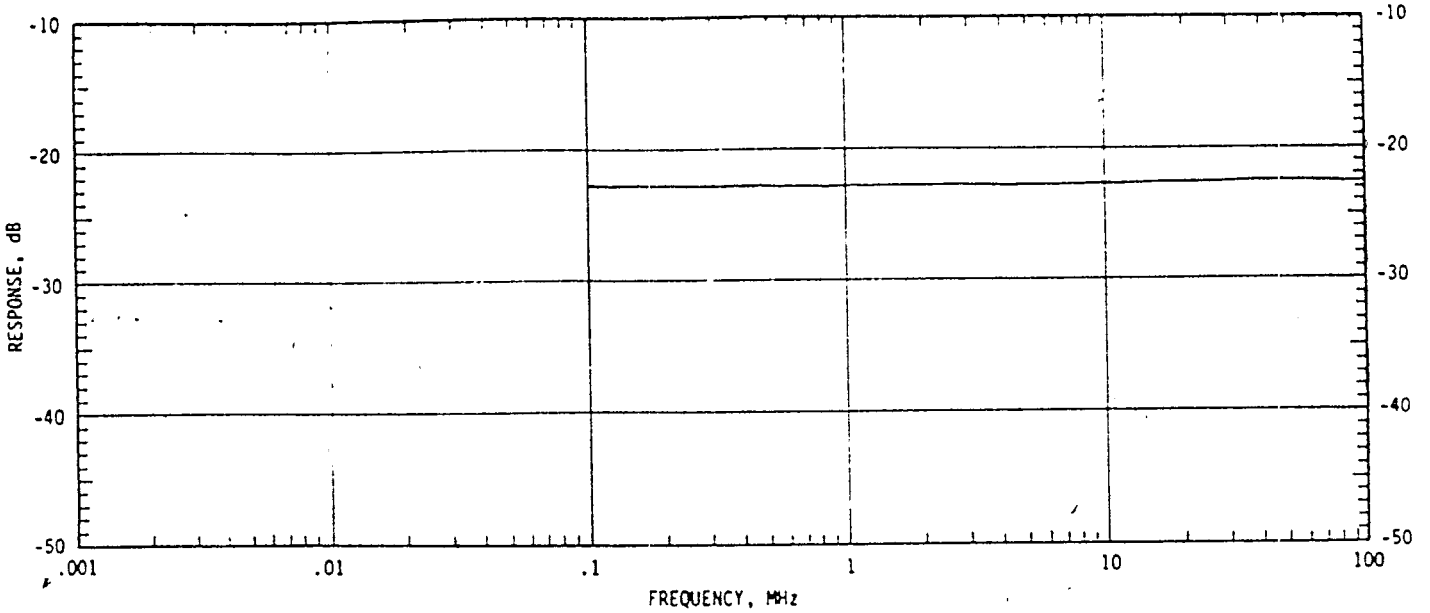


Figure 16. Frequency response for Fisher prototype F32-8 current sensor (not corrected for cable length).

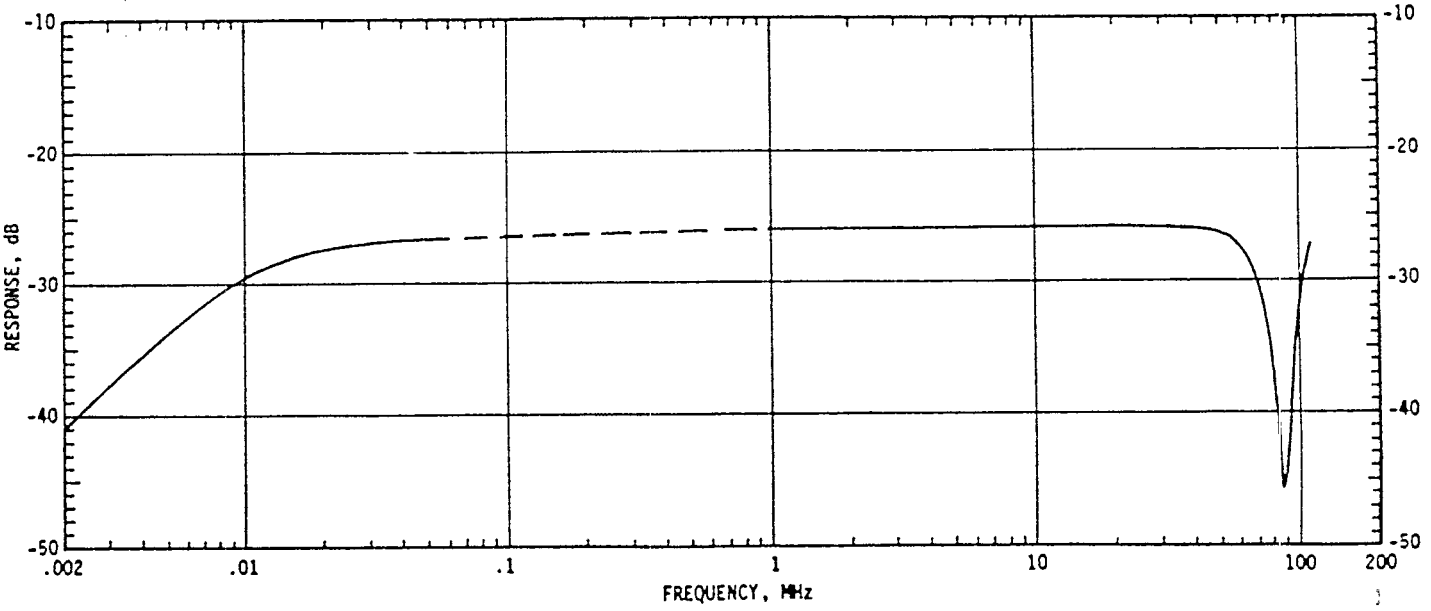


Figure 17. Frequency response for SEC-X1 current sensor (not corrected for cable length).

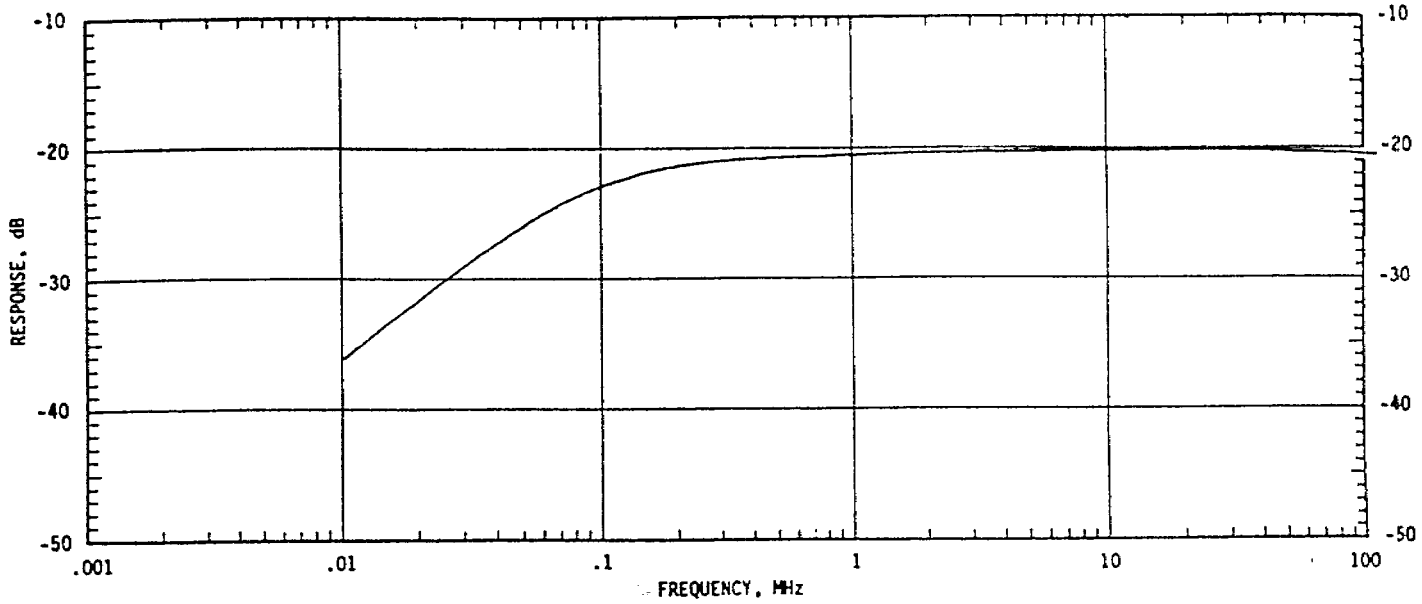


Figure 18. Frequency response for SCI-X1 current sensor (corrected for 22.1 foot cable length).

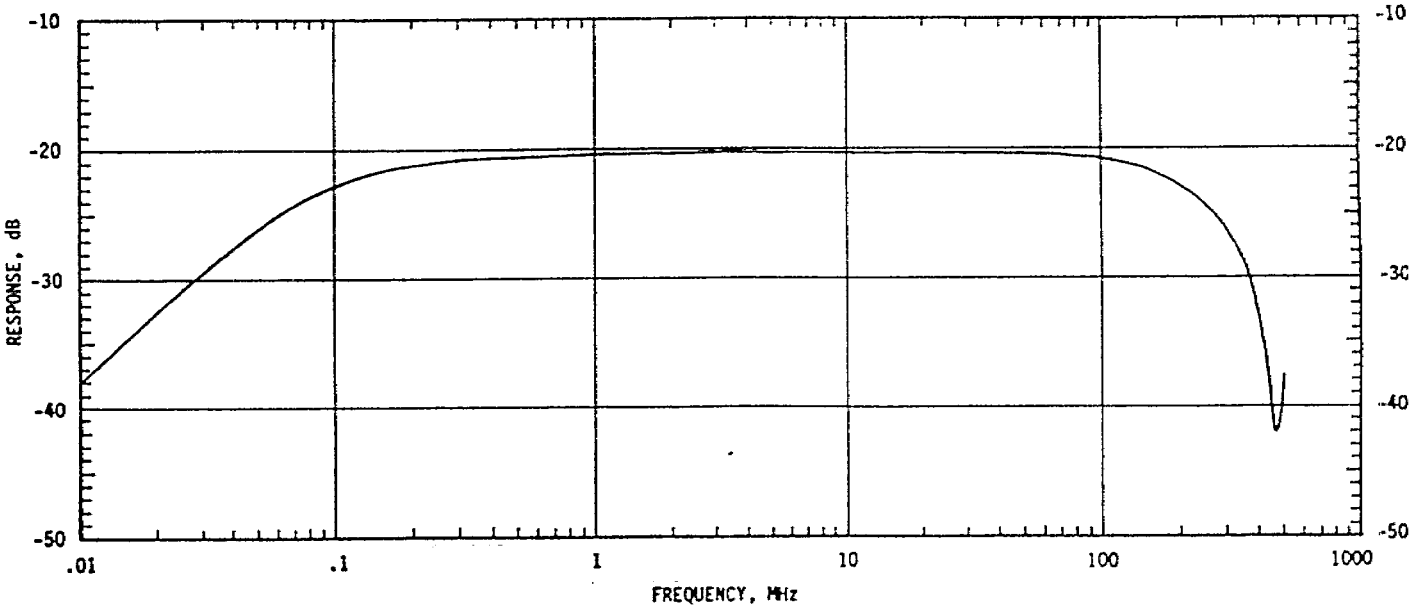


Figure 19. Frequency response for ICI-X3A current sensor (not corrected for cable length).

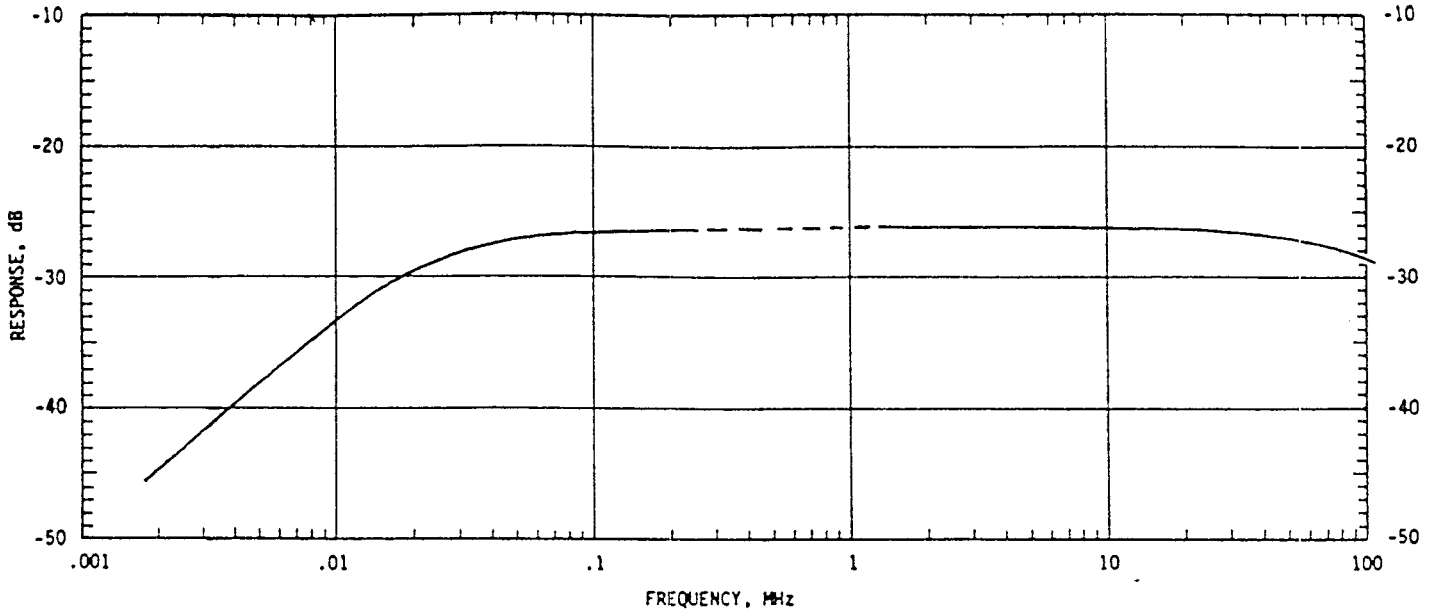


Figure 20. Frequency response for ICI-X3B current sensor (corrected for 16.7 foot cable length).

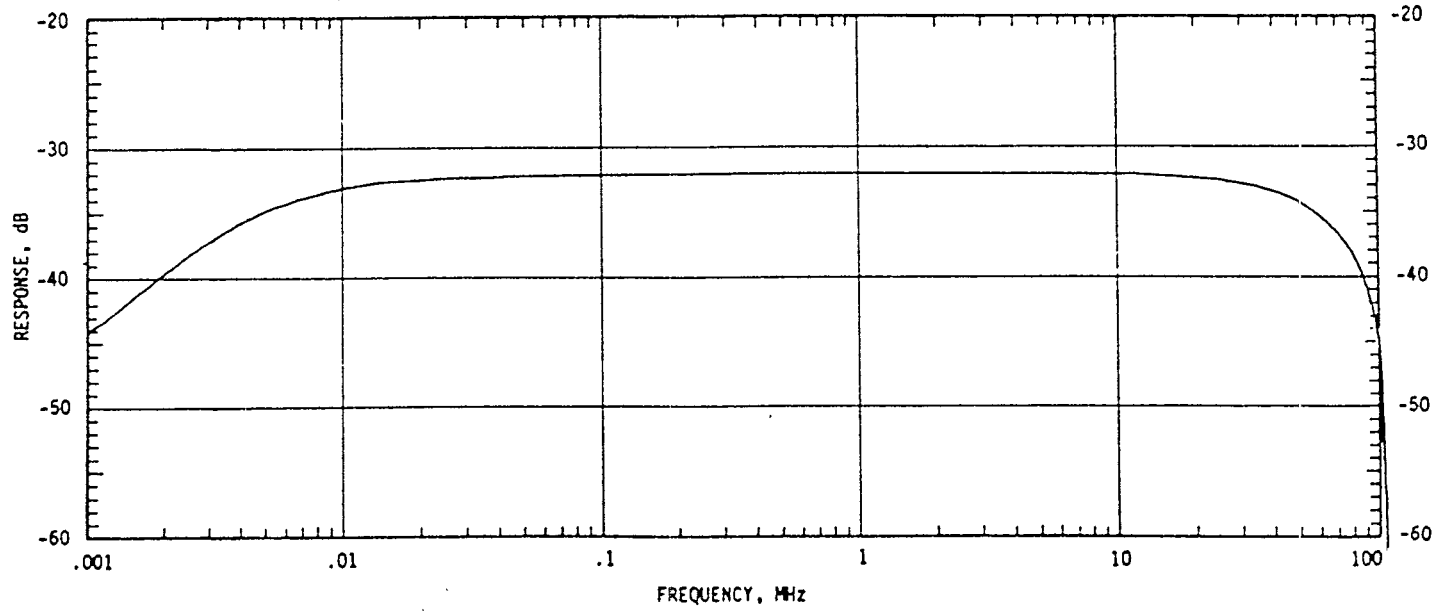


Figure 21. Frequency response for ICI-X3C current sensor (corrected for 17.5 foot cable length).

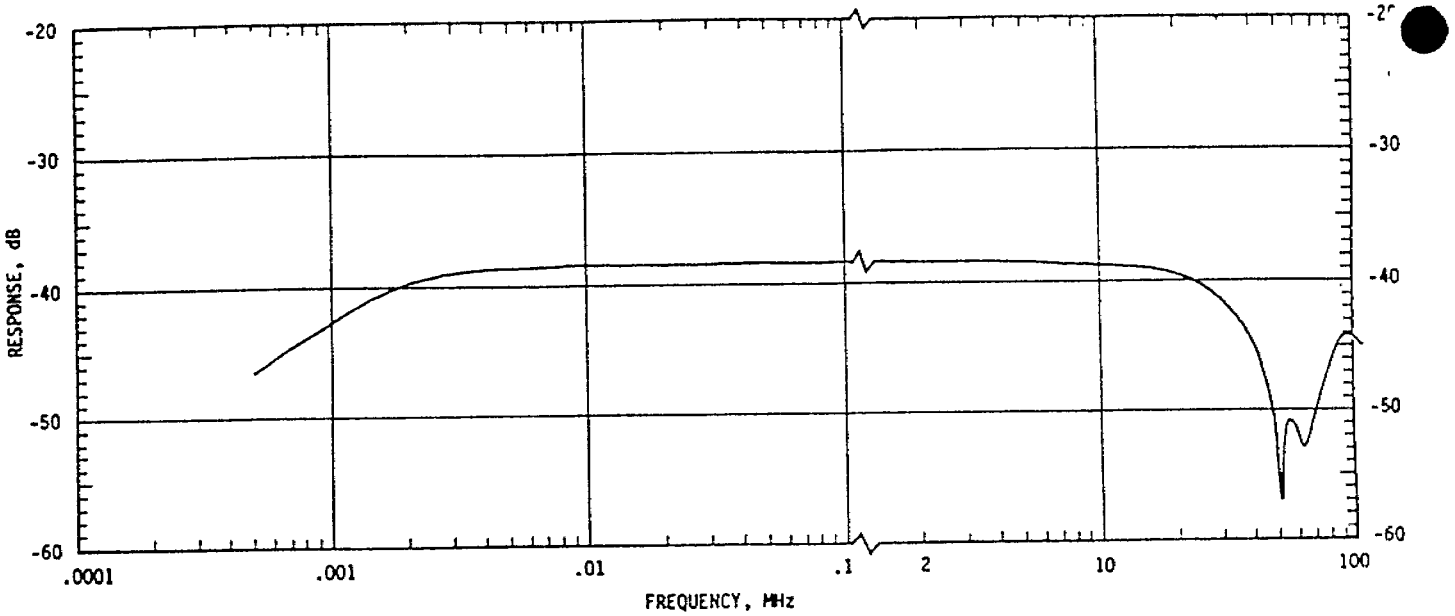


Figure 22. Frequency response for ICI-X3D current sensor (not corrected for cable length).

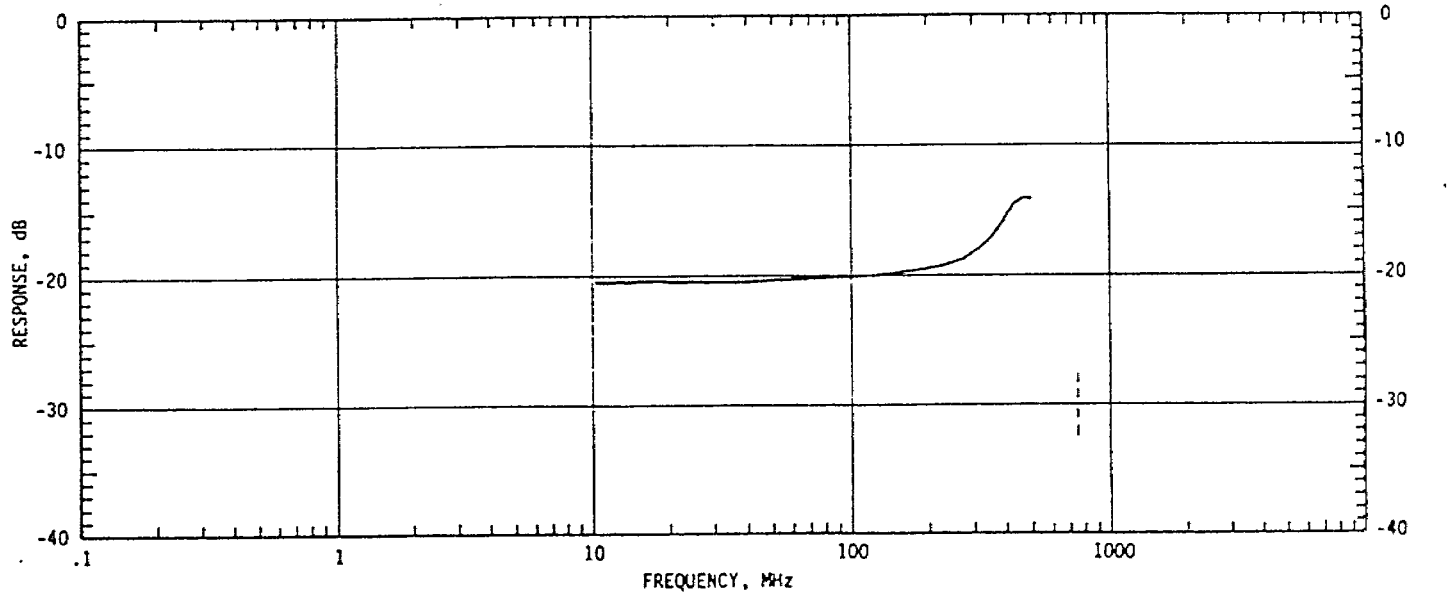


Figure 23. Frequency response for SCI-XI current sensor (corrected for 19.20 foot cable length).

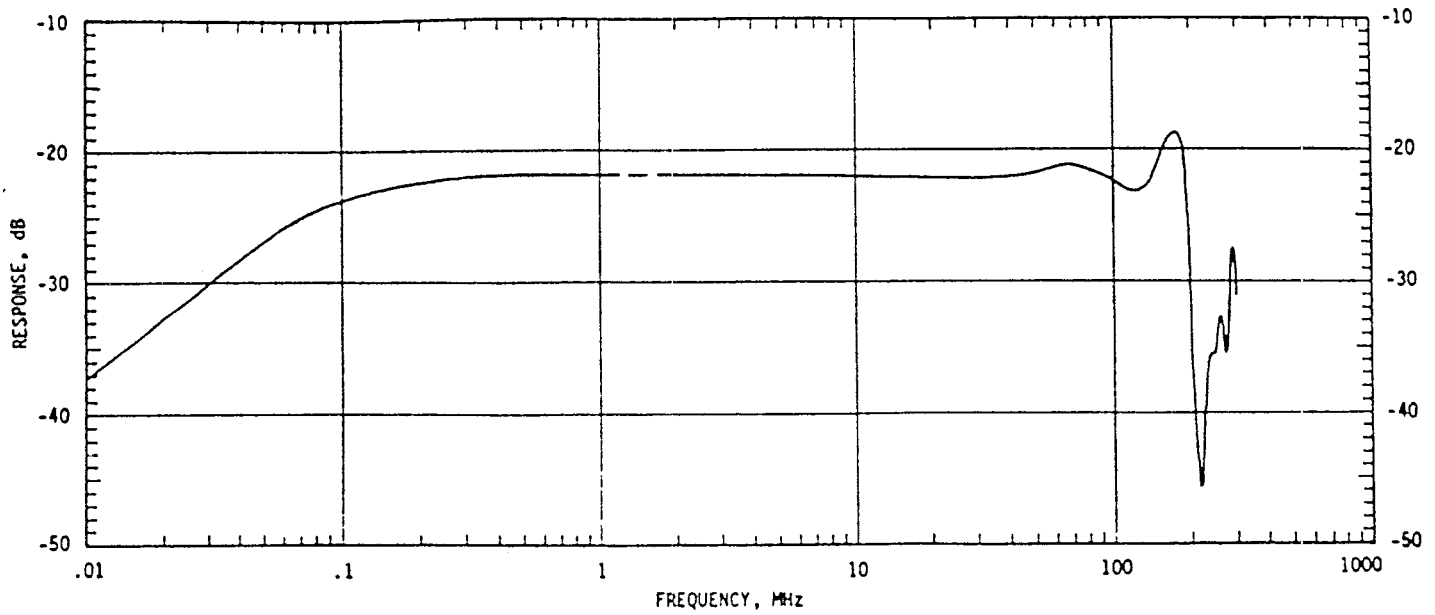


Figure 24. Frequency response for F32-9 current sensor (corrected for 26.8 foot cable length).

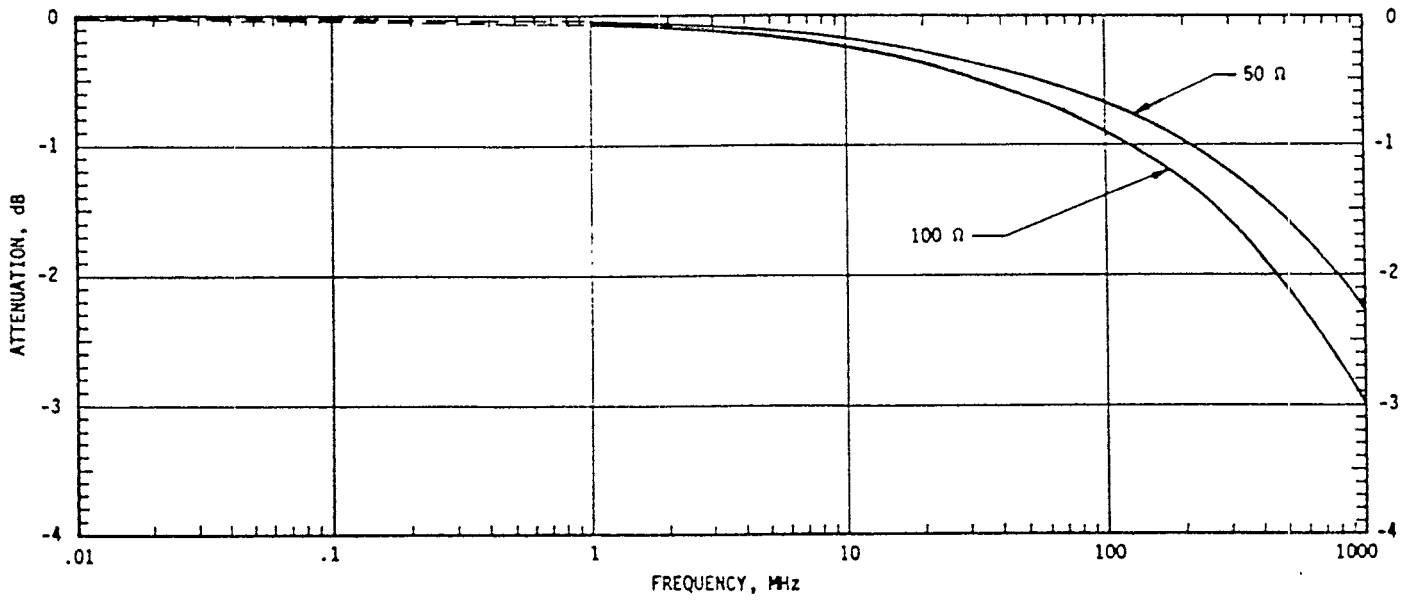


Figure 25. Attenuation as function of frequency for ten (10) foot lengths of aluminum coaxial cable with teflon dielectric.

SECTION 5

# SENSOR MAINTENANCE

## 5-1 METHOD

The integrity of most sensors can be verified by a time domain reflectometer (TDR) test. This test examines the reflection of a square wave by impedance variations in the coaxial line. A careful comparison of the TDR with a TDR standard (one for each sensor type) will show that the sensor is operational. The TDR used for the test must have the same risetime characteristics as the TDR used for the standard, and in differential sensors the second coaxial line should be terminated in its characteristic impedance (50 Ω for the sensors discussed in this report). It should be noted that a TDR of a PMD sensor will show an open at the sensor and will not verify sensor integrity.

## 5-2 HURON KING SENSOR TDR LOG

Figures 26 through 38 are TDR photos for 13 of the HURON KING current sensors. The information contained in this section should be treated as preliminary as it may be amended should further more accurate information become available.

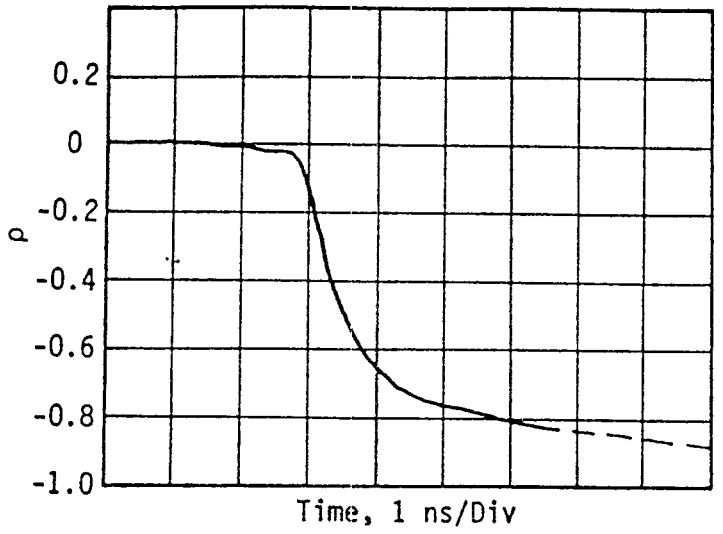


Figure 26. TDR response for CML-X3 current sensor.

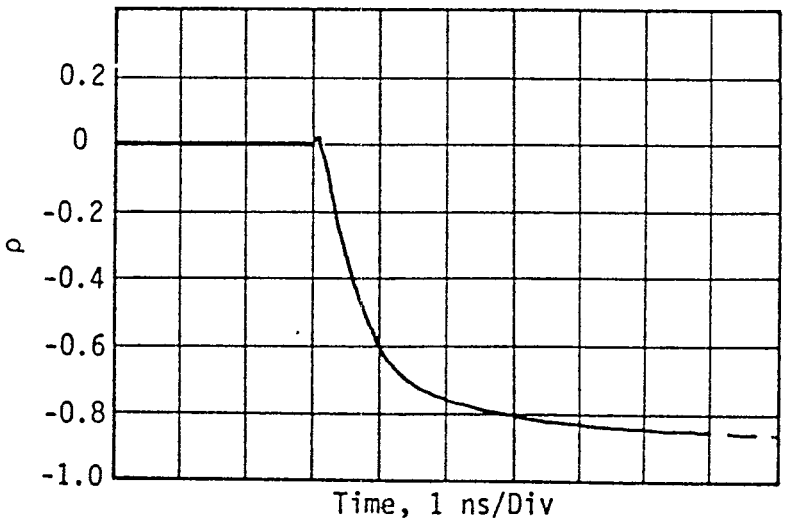


Figure 27. TDR response for RML-X1 current sensor.

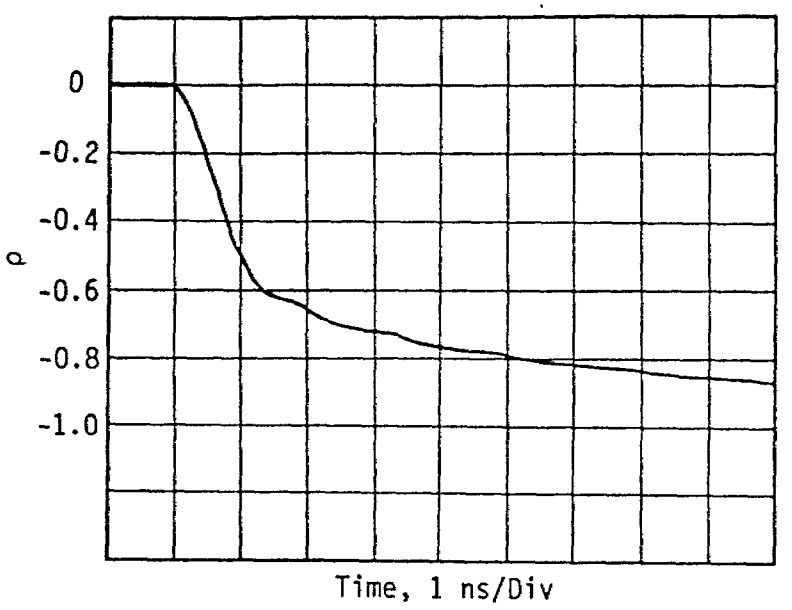


Figure 28. TDR response for OMM-4 current sensor.

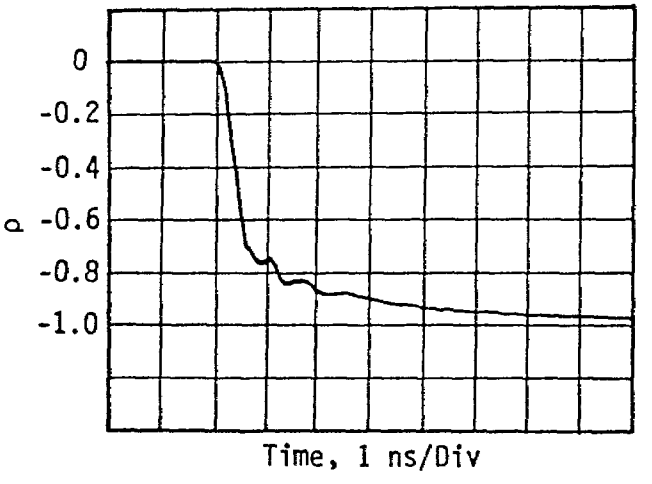


Figure 29. TDR response for SMM-1 current sensor.

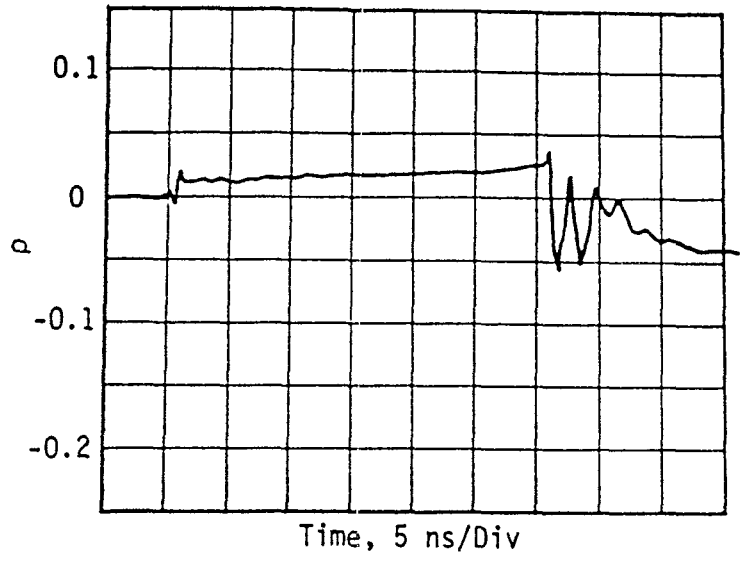


Figure 30. TDR response for ICI-X2 current sensor.

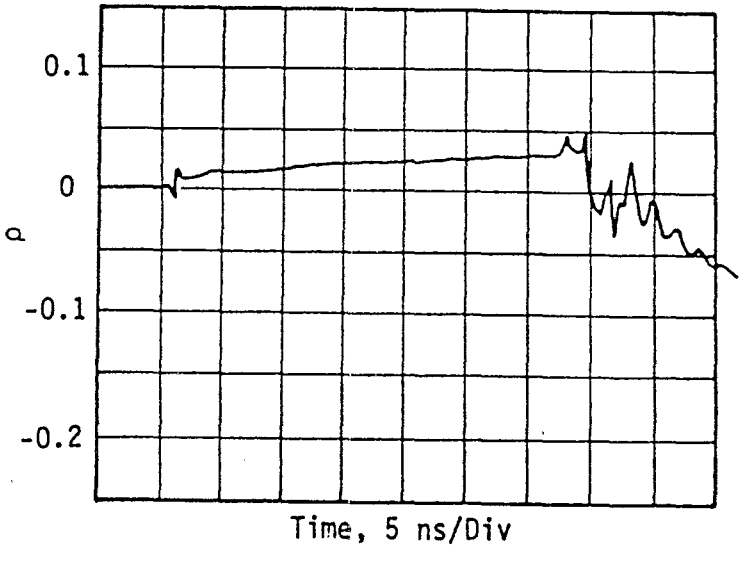


Figure 31. TDR response for ICI-X3A current sensor.

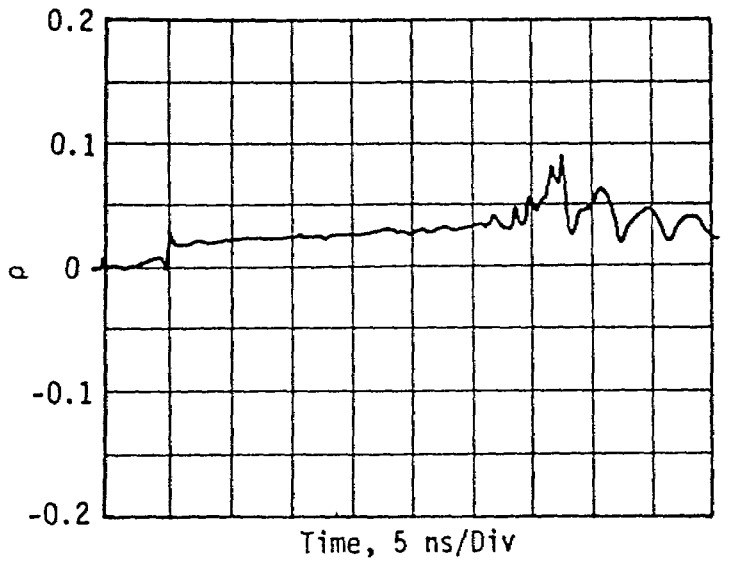


Figure 32. TDR response for ICI-X3B current sensor.

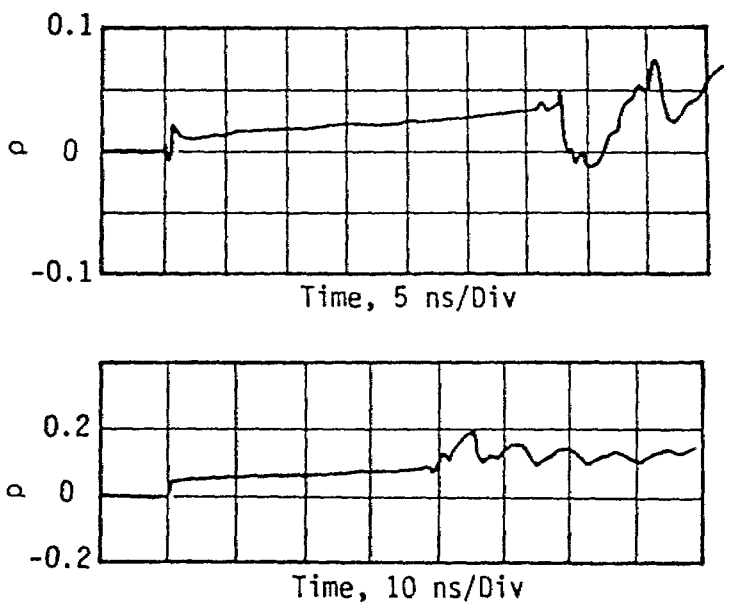


Figure 33. TDR response for ICI-X3C current sensor.

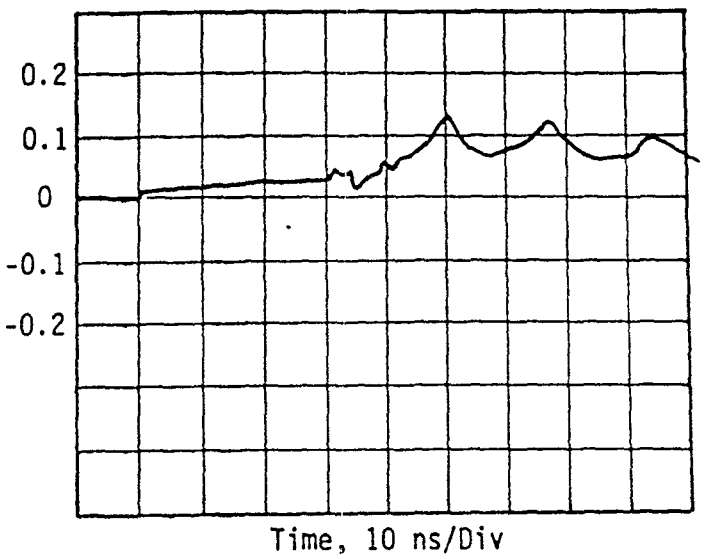


Figure 34. TDR response for ICI-X3D current sensor.

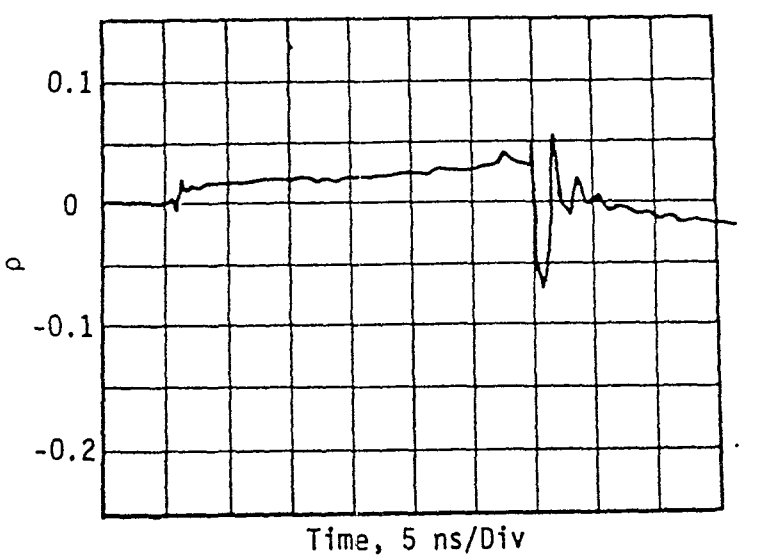


Figure 35. TDR response for SCI-X1 current sensor.

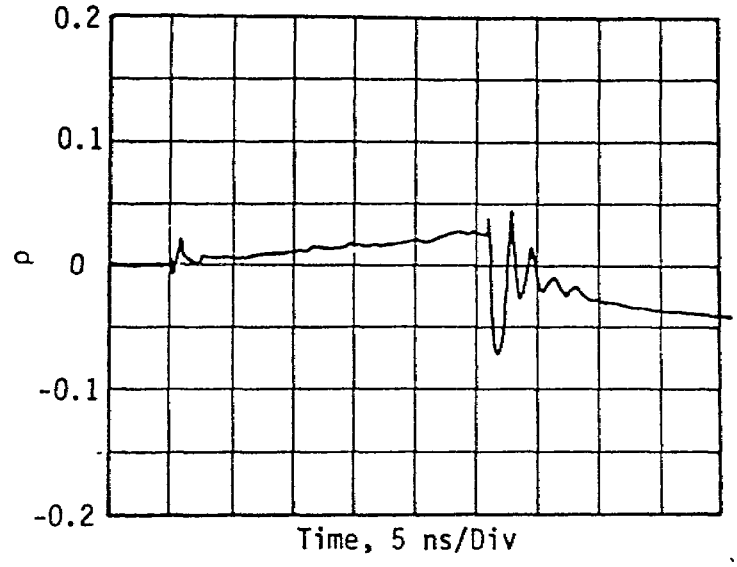


Figure 36. TDR response for SCI-X2 current sensor.

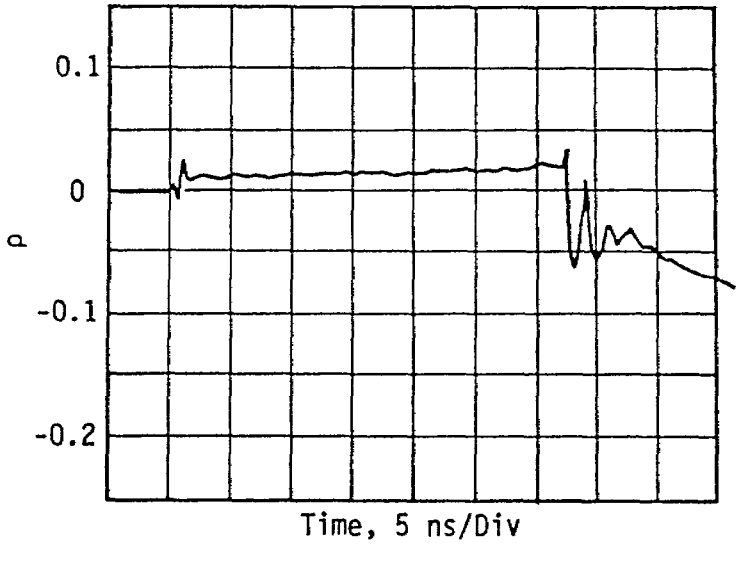


Figure 37. TDR response for SCI-X3 current sensor.

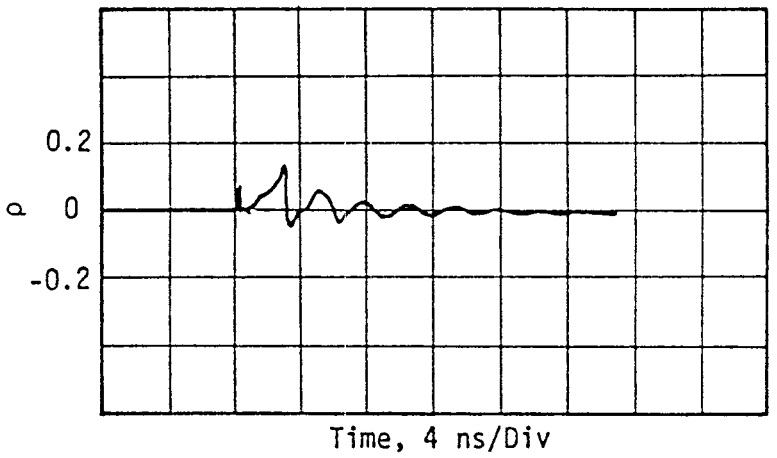


Figure 38. TDR response for SCI-X4 current sensor.

# SECTION 6

# CONCLUSIONS

The post shot analysis of the underground test data indicates that the grounding and shielding implementation achieved an excellent signal to noise ratio and a high percentage of data return. All the sensors performed well in this high noise environment. The new developments in the B-dot sensors resulted in a thin ground plate that had a minimal enhancement of the magnetic field and allowed measurements between two conducting surfaces. Changing the position of the sensing gap on the I-dot (SMM) sensor provided greater flexibility in location in a complex physical geometry. The development of small split core current sensors utilizing a balanced transmission line as the pickup winding resulted in improved bandwidth and superior noise rejection. The noise rejection capability of the differential probes is useful in many high noise environments.

# REFERENCES


1. AFWL-TR-69-58, Vols I and II, Development of Hardened Magnetic Field Sensors, Oct 69.

2. CSC II/3-E-031, Cylindrical Moebius Loop Radiation Hardened B-Dot Sensor (CML-X3A(R) & CML-X5A(R)) Development, 15 Jun 76.

3. Baum, C.E., Maximizing Frequency Response of a B-Dot Loop, Sensor & Simulation Notes, Note 8, 9 Dec 64.

4. CSC II/3-E-033, Parallel Mesh Dipole Radiation Hardened E-Field Sensors (PMD-1C) Development, 30 June 76.

5. CSC II/3-E-176, R&D on the Parallel Mesh Dipole Sensor (PMD), Jun 77.

6. CSC II/3-E-032, Outside Moebius Mutual Radiation Hardened I-Dot Sensor (OMM-2A) Development, 30 Jun 76.

7. Baum, C.E., Some Considerations for Inductive Current Sensors, Sensor & Simulation Notes, Note 59, 8 Jul 68.

8. Grossner, N.R., Transformers for Electric Circuits, McGraw-Hill, 1967.

9. Baum, C.E., Characteristics of the Moebius Strip Loop, Sensor & Simulation Notes, Note 7, 3 Dec 64.